Catena 238 (2024) 107835

Contents lists available at ScienceDirect

Catena

journal homepage: www.elsevier.com/locate/catena

Exploring the geomorphological adequacy of the landslide susceptibility maps: A test for different types of landslides in the Bidente river basin (northern Italy)

Chiara Martinello [a], Michele Delchiaro [b,*], Giulia Iacobucci [b], Chiara Cappadonia [a], Edoardo Rotigliano [a], Daniela Piacentini [b]

[a] Department of Earth and Marine Sciences (DiSTeM), University of Palermo, Via Archirafi 22, 90123 Palermo, Italy
[b] Department of Earth Sciences, Sapienza University of Rome, Piazzale Aldo Moro 5, 00184 Rome, Italy

ARTICLE INFO

Keywords:
Landslide susceptibility
WoE
MARS
Predisposing factors
Variable importance
Northern apennines

ABSTRACT

Landslide susceptibility modelling is a crucial tool for implementing effective strategies in landslide risk mitigation. A plethora of statistical methods is available for generating accurate prediction images; however, the reliability of these models in terms of geomorphological adequacy is often overlooked by scholars. This critical flaw may result in concealed prediction errors, undermining the trustworthiness of the obtained maps. A key aspect of evaluating the geomorphological soundness of these models lies in factor analysis, specifically considering the correlation of explanatory variables with the final susceptibility score rather than solely focusing on their impact on model accuracy.

This study delves into research conducted in the Bidente river basin (Italy) that analyes results obtained from slide, flow, and complex susceptibility models using Weight of Evidence (WoE) and Multivariate Adaptive Regression Splines (MARS) statistical methods. The research critically examines each factor class's role in defining susceptibility scores for different landslide typologies. The comparison between susceptibility maps generated by WoE and MARS for each typology (slide = 0.78; flow = 0.85; complex: 0.79) (slide = 0.78; flow = 0.85; complex: 0.79)reveals good to excellent prediction skill, with MARS demonstrating a 5 % higher performance index.

The study emphasises the importance of spatial relationships between variables and landslide occurrences, highlighting that individual classes of variables influence the final susceptibility score based on their combined role with other predictor classes. In particular, in this study, results highlight that lithotecnical and landform classification classes delimit the landslide domain, while topographic attributes (steepness, curvatures, SPI and TWI) modulate the score inside. The proposed approach offers insights into investigating the geomorphological adequacy of landslide prediction images, emphasising the significance of factor analysis in evaluating model reliability and uncovering potential errors in susceptibility maps.

1. Introduction

Landsliding is a major slope modelling process in response to slope gravitational instabilities that contributes to hillslope erosion (Montgomery and Dietrich, 1994; Roering et al., 2001) and it constitutes a severe environmental hazard with large-scale social, economic, and natural impact (Guzzetti et al., 1999; Parise and Jibson, 2000;Pourghasemi and Rahmati, 2018, Rouhi et al., 2019, 2022). In this regard, landslide susceptibility maps are key tools for land-use planning, management, and risk mitigation, since they depict the spatial probability of landslide occurrence, based on local terrain conditions (Brabb, 1984; Guzzetti et al., 1999, 2005; Mergili et al., 2014; Martinello et al., 2021, 2022a,b; Bufalini et al., 2021).

Many different approaches and methods have been proposed to ascertain landslide susceptibility. Among them, statistical modelling is based on the hypothesis that the same environmental conditions that caused landslide occurrence in the past will lead to slope failures also in the future. Hence, the generation of a landslide model requires the

* Corresponding author.
E-mail address: michele.delchiaro@uniroma1.it (M. Delchiaro).

https://doi.org/10.1016/j.catena.2024.107835
Received 2 August 2023; Received in revised form 6 January 2024; Accepted 16 January 2024
Available online 23 January 2024
0341-8162/© 2024 The Author(s). Published by Elsevier B.V. This is an open access article under the CC BY license (http://creativecommons.org/licenses/by/4.0/).

definition of explanatory variables that reflect the pre-failure characteristics of the slopes (Carrara, 1983; Chacón et al., 2006; Guzzetti et al., 1999; Huabin et al., 2005; Van Westen et al., 2008).

According to the review of Reichenbach et al. (2018), the most important "explanatory thematic variables", here after named also "independent variables" or "predictors" or "covariates", can be grouped in: i) morphological (e.g., slope, aspect, elevation, relief, curvature), ii) geological (geo-lithological, distance to fault, geo-structural), iii) land cover (land use, soil type, vegetation cover, distance to road) and iv) other (precipitation, recorded or expected seismic acceleration, geotechnical properties etc.). In general, topography (slope, aspect, relief, curvature, etc.) and lithology are considered conditioning (preparatory and predisposing, e.g. Delchiaro et al., 2023; Discenza et al., 2023) factors (e.g., Pourghasemi and Rahmati, 2018; Delchiaro et al., 2021), while rainfall, earthquakes, and anthropogenic stresses (e.g, road undercutting) are known as triggering factors (e.g., Lee et al., 2008; Tanyaş et al., 2022a, 2022b). However, as regards rainfall, depending on the duration of the time window it can be also considered as a predisposing variable.

In general, the inferential study between the dependent and independent variables can be performed with simple bivariate to sophisticated multivariate and machine learning approaches. In detail, in bivariate statistical analysis, landslide incidence is computed separately on each explanatory variable and then using normalized values (landslide density per parameter class in relation to the landslide density over the whole area), a total susceptibility map can be created by the addition of the weights for each individual factor class. The most important bivariate methods surely include Frequency Ratio (FR, e. g., Lee and Pradhan, 2007; Yilmaz, 2009; Delchiaro et al., 2021) and Weights of Evidence (WoE, e.g., Lee and Choi, 2004; Piacentini et al., 2012; Ilia and Tsangaratos, 2016) models. Conversely, the multivariate analysis focuses on the relations between multiple variables whose role in explaining a given past landslide scenario is examined simultaneously. Logistic regression (e.g., Costanzo et al., 2014), Maximum Entropy Algorithm (MaxEnt; e.g., Lombardo et al., 2016), Generalized Linear Model (GLM; e.g., Atkinson & Massari, 1998), Artificial neural networks (ANN; e.g., Ripley, 1996), Support Vector Machine (SVM; e.g., Huang & Zhao, 2018), Random Forests (RF; e.g., Sun et al., 2020) and (MARS, e. g., Vargas-Cuervo et al., 2019) are among the most exploited multivariate methods.

A great number of papers dealing with methods comparison have been published in recent years (e.g., Pradhan, 2010; Vorpahl et al., 2012; Al-Najjar et al., 2021; Pandey et al., 2023). However, in almost all the cases, the comparison is limited in indicating best/worst performances and/or selected/unselected factors with a totally lacking geomorphological interpretation of the obtained results (i.e., how do different landslide types result in different models and accuracies?).

At the same time, the importance of the variables and how to investigate them is a topic that still deserves further investigation.

In fact, various methods exist for quantifying the incidence of factors in the optimised predictive models, including: Fuzzy-Rough sets (e.g., Gorsevski and Jankowski, 2008, 2010); Chi-square (e.g., Kutlug Sahin et al., 2017); Fisher (e.g., Kutlug Sahin et al., 2017); Relief (e.g., Kutlug Sahin et al., 2017); Information Gain (e.g., Chen et al., 2018); Information Gain Ratio (Tien Bui et al., 2016; Zhou et al., 2018); the mean value of relative contribution (e.g., Huang et al., 2020); permutation-based variable accuracy importance methods (e.g., Zhao et al., 2022). However, all these methods are focused on estimating the incidence of the predictors in controlling the model accuracy, strongly relying their results on the statistical evaluation of the model performance. In this way, weak attention is given to the geomorphological adequacy of the obtained susceptibility classes (i.e., with a focus on the importance of the single class of variables in relation to the final susceptibility score).

This lack of geomorphological adequacy in the evaluation of the model performance takes an even more critical impact when mixed landslide inventories are used for calibration, without clearly splitting the mapped cases according to the landslide typology. This same condition has consequences both in terms of the reliability of the obtained predictive maps and the subtending variable importance.

To explore the above-mentioned topics, geomorphological adequacy is here investigated for slide, flow and complex landslide types in the Bidente river basin, using two statistical methods: Weight of Evidence (WoE; Bonham-Carter, 1989) and Multivariate Adaptive Regression Splines (MARS; Friedman, 1991). In particular, the model comparison for the three different landslide typologies and the two methods was performed from a geomorphological perspective by investigating the multivariate score distribution inside each factor class. Besides, the comparison between the two susceptibility maps obtained for each landslide typology by applying the two methods is performed for score classes so to estimate the general congruence of the prediction images.

2. Physical setting of the study area

The Bidente river basin lies in the Romagna Apennines, spanning approximately from 43°50′00′' N to 44°20′00′'N. It encompasses the northeastern slope of the mountain range and flows mainly northeastward. Its headwater is located at the Apennines drainage divide between Toscana and Emilia Romagna regions. At this point, three different rivers are originated, Bidente di Corniolo, Bidente di Ridracoli, and Bidente di Pietrapazza, whose join upstream of Santa Sofia village generates the Bidente River (Fig. 1).

The Bidente River ends near Meldola village, where it becomes the Ronco River. The Bidente drainage area is about 600 km^2, with a difference in height of about 1600 m. Indeed, the study area is essentially mountainous and hilly, except for the area downstream of Meldola village.

The region is characterized by a cool temperate climate setting in the inner mountainous part of the basin, while the hilly sector proximal to the Po Plain is subcontinental (Antolini et al., 2015; Nistor, 2016). The mean annual precipitation is 1305 mm in the mountainous sector and 780 mm in the plain downstream of Meldola, with the highest values in autumn and spring; the mean temperature is 11 °C in the inner sector and 14 °C along the plain, with the minimum in January and the maximum in July and August (Antolini et al., 2017).

The selected study area for about 50 % is occupied by woodlands upstream of Cusercoli village, while the hilly and valley sector northeastward holds farming and industrial activities, as well as the highest number of settlements (https://geoportale.regione.emilia-romagna.it/catalogo/dati-cartografici/pianificazione-e-catasto/uso-del-suolo/layer-9).

2.1. Geological and geomorphological features

The Romagna Apennines belongs to the Tertiary fold-and-thrust Apennine belt, developed since the Late Cretaceous due to the subduction of Adria beneath Europe (Picotti and Pazzaglia, 2008; Wegmann and Pazzaglia, 2009, Ponza et al., 2010; Ghiselli et al., 2011; Carminati and Doglioni, 2012; Gunderson et al., 2014). About 4 Ma, the Apennine wedge emerged above sea level and its uplift and exhumation increased during the Plio-Pleistocene (Bartolini, 2003; Picotti and Pazzaglia, 2008; Ponza et al., 2010). The rock uplift is still active as noticed by seismicity (Di Bucci and Mazzoli, 2002; Pondrelli et al., 2006; Ponza et al., 2010), GPS-geodesy (Serpelloni et al., 2005), and geomorphic evidence of growing folds and faults (Picotti and Pazzaglia, 2008). As reported in Picotti and Pazzaglia (2008, and reference therein), although the total convergence rate is 8–10 mm/yr, the pace of subduction remains relatively slow at 4–5 mm/yr, constituting half of the overall convergence rate.

The upper two third of the Bidente basin is mainly constituted by the Marnoso-Arenacea Fm (FMA), the Miocene thick siliciclastic turbidite complex mainly derived from the Alps and distinguished in numerous members (Conti et al., 2020; https://ambiente.regione.emilia-romagna.

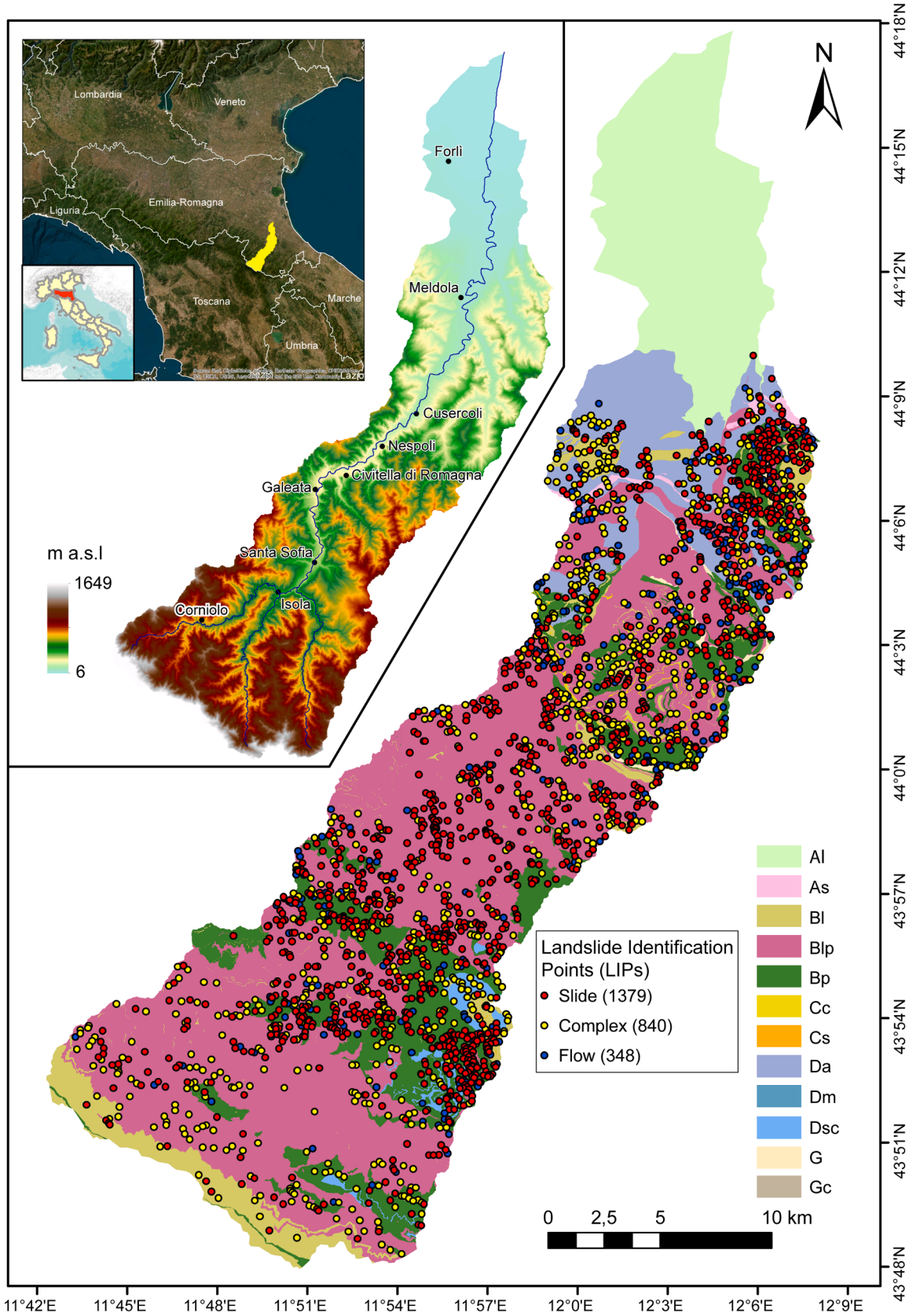

Fig. 1. The Bidente River basin: Digital Elevation Model with 10 m of spatial resolution and the lithotechnical map with the location of slides, flows and complex landslides. Lithotechnical units: Al - Alluvial plain deposits; As - stratified massive rocks; Bl – sandstone(S)/pelitic(P) alternations with S/P > 3; Blp - sandstone/pelitic alternations with 0.3 < S/P < 3; Bp - sandstone/pelitic alternations with S/P < 0.3; Cc - clast-supported conglomerates; Cs – weakly-cemented sands; Da - consolidated clays; Dm - marls; Dsc - tectonized clays and argillites; G - gypsums; Gc - gypsums in chaotic deposits (Lithotechnical map of Emilia Romagna https://ambiente.regione.emilia-romagna.it/en/geologia/geology/land-instabilities/img/litotecnica.jpg).

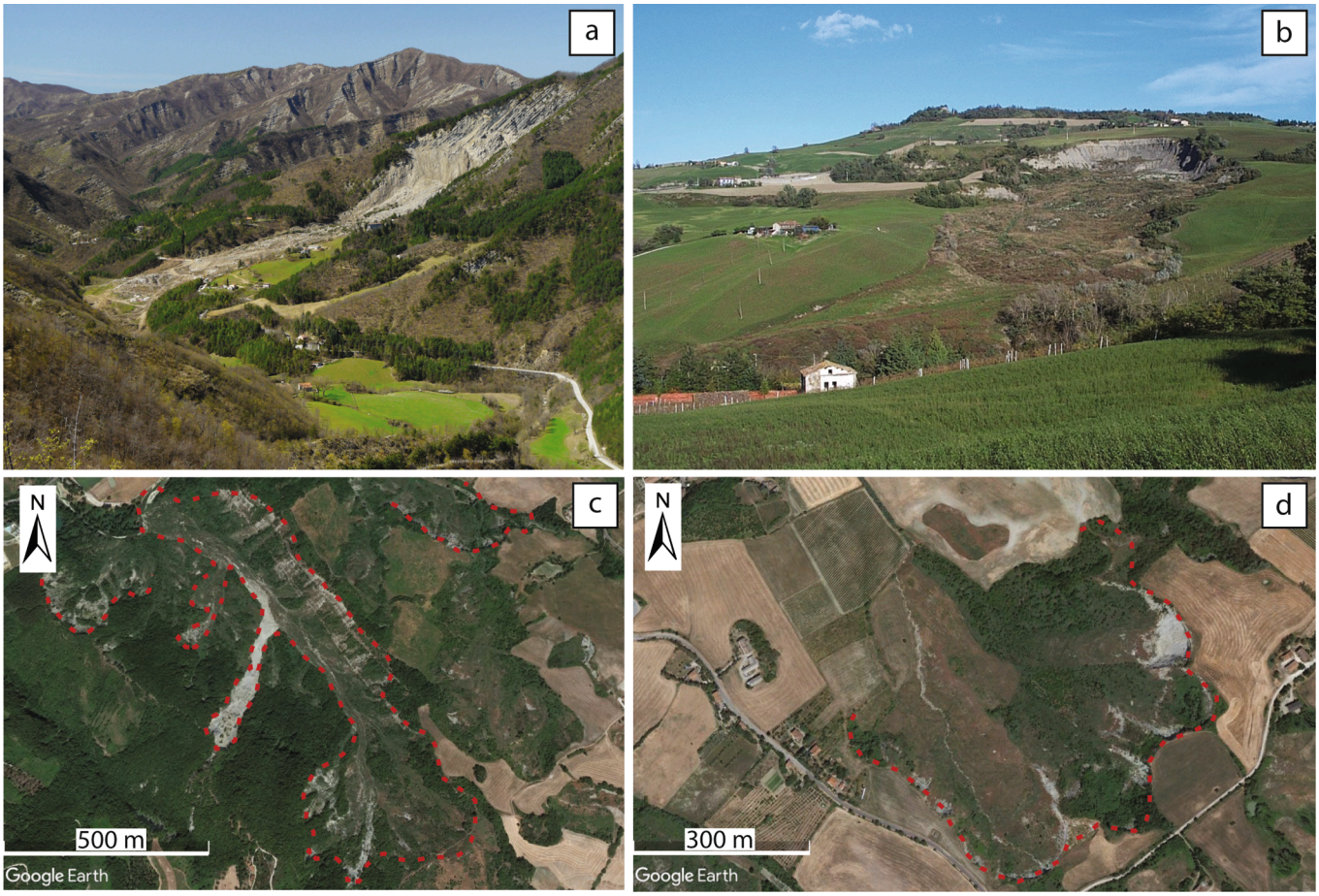

Fig. 2. Examples of landslides occurring in the study area: a) Poggio Baldi rockslide (March 18, 2010; Piacentini et al., 2018); b) the roto-translational slide near Civitella di Romagna (May 2017; https://ambiente.regione.emilia-romagna.it/en/geologia/geology/land-instabilities/le-caratteristiche-dei-fenomeni-franosi-in-emilia-romagna); c and d) the satellite views of several flows near Cusercoli.

it/it/geologia/geologia/geologia-emilia-romagna/geologia-dellappennino-emiliano-romagnolo). While, the downstream sector preserves the Upper Miocene-Pliocene sequence, mainly consisting of the Colombacci Fm (FCO), Argille Azzurre Fm (FAA), and limited outcrops of the Ghioli di Letto Fm (GHL), Tetto Fm (GHT), and the Gessoso-Solfifera Fm (GES) (Wegmann and Pazzaglia, 2009; Conti et al., 2020; https://ambiente.regione.emilia-romagna.it/en/geologia/geology/land-instabilities/img/).

The variability in outcropping formations, such as the alternation of soft and hard rock types, from thinly layered to massive (Piacentini et al., 2018), let us consider the lithotechnical units reported in Fig. 1. In detail, twelve lithotechnical units can be distinguished in the Bidente basin. Notably, the "Al" unit (alluvial plain deposits) is specifically included to classify the alluvial deposits of the Po Plain located downstream of Meldola. More than 50 % of the study area has been classified as "Blp" (massive\pelitic alternations with $0.3 < S\backslash P < 3$), followed by "Bp" (massive\pelitic alternation with $S\backslash P < 0.3$; 15 %), "Al" (14 %), "Da" (consolidated clays; 8.5 %), and "Bl" (massive\pelitic alternation with $S\backslash P > 3$; 6.5 %). The remaining units ("As", "Cc", "Cs", "Dm", "Dsc", "G", and "Gc") constitute the 5 % of the study area.

The Bidente basin is oriented parallel to the orogenic slope and perpendicular to the main structural grain (Wegmann and Pazzaglia, 2009). Here, about 13 % of the study area is affected by landslides, where the most common type is slides, followed by complex and flow types that involve both earth and rock masses (Piacentini et al., 2018). Despite large landslides are quite frequent in the Emilia Romagna region, which results as one of the most landslide susceptible regions worldwide (Bertolini et al., 2005; Generali and Pizziolo, 2013; Pizziolo et al., 2014; Triglia et al., 2015; Piacentini et al., 2018). The most frequently recognized landslides are relatively small and shallow (Piacentini et al., 2018), occurring over near one-fifth of the hilly and mountainous sector (Bertolini et al., 2005). As reported in Bertolini et al. (2005), although the largest landslides in the Emilia Romagna were originated as earthflows after the Last Glacial Maximum (LGM), intense and\or long rainfalls, often combined with snowmelt, can play a key role as triggering factors for the activation and re-activation of mass movements (Bertolini et al., 2005; Montrasio et al., 2012; Pizziolo et al., 2014; Piacentini et al., 2018).

2.2. Landslide inventory

The dataset used in this study was obtained from the Geological Survey of the Emilia Romagna. It includes landslide deposits originating from the Quaternary deposits of the Emilia-Romagna Geological Map at a scale of 10,000. Additionally, information from the Landslide Historical Archive (https://ambiente.regione.emilia-romagna.it/it/geologia/geologia/dissesto-idrogeologico/larchivio-storico-dei-movimenti-franosi) and the Landslides inventory maps of the Emilia-Romagna Region (https://ambiente.regione.emilia-romagna.it/it/geologia/geologia/dissesto-idrogeologico/la-carta-inventario-delle-frane) were also incorporated.

The geological survey for landslide mapping was initially carried out between 1980 and 2000, and later revised for the IFFI project (Landslide inventories in Italy - Inventario dei Fenomeni Franosi in Italia) (https://ambiente.regione.emilia-romagna.it/it/geologia/geologia/dissesto-idrogeologico/la-carta-inventario-delle-frane). The field

Table 1
Codes and description of the classes proposed for each geo-environmental variable selected for the study.

Variable	Acronym of the class	Units	Description/ Numerical interval
ELE	**1**	m (a.s.l.)	<27
	2		>=27 & <371
	3		>=371 & <500
	4		>=500 & <754
	5		>= 754
PLC	**1**	rad/m	<−0.10
	2		>=−0.10 & <−0.027
	3		>=−0.027 & <0.027
	4		>=0.027 & <0.10
	5		>=0.10
PRF	**1**	rad/m	<−0.002
	2		>=−0.002 & <−0.0013
	3		>=−0.0013 & <0.0013
	4		>=0.0013 & <0.002
	5		>=0.002
SLO	**1**	degree	<5
	2		>=5 & <10
	3		>=10 & <15
	4		>=15 & <20
	5		>=20 & <25
	6		>=25 & <30
	7		>=30 & <35
	8		>=35 & <40
	9		>=40 & <45
	10		>=45
SPI	**1**	kg m^2 s^{-3}	<0.4
	2		>=0.4 & <184.8
	3		>=184.8 & <185.7
	4		>=185.7 & <20605.7
	5		>20605.7
TWI	**1**	m	<5.73
	2		>=5.73 & <7.59
	3		>=7.59 & <8.29
	4		>=8.29 & <10.42
	5		>=10.42
ASP	**N**	degree	0–22.5 & 337.5–360
	NE		22.5–67.5
	E		67.5–112.5
	SE		112.5–157.5
	S		157.5–202.5
	SW		202.5–247.5
	W		247.5–292.5
	NW		292.5–337.5
LCL	**Ca**		Canyon
	Md		Midslope drainage
	Hw		Headwater
	Uv		U-shaped valley
	Pl		Plains
	Os		Open slope
	Us		Upper slope
	Lr		Local ridge
	Mr		Midslope ridge
	Mt		Mountain tops
LITO	**Al**		Alluvial plain deposits
	As		Stratified massive rocks
	Bl		Sandstone/pelitic alternations with S/P > 3
	Blp		Sandstone/pelitic alternations with 0.3 < S/P < 3
	Bp		Sandstone/pelitic alternations with S/P < 0.3
	Cc		Clast-supported conglomerates
	Cs		Weakly-cemented sands
	Da		Consolidated clays
	Dm		Marls
	Dsc		Tectonized clays and argillites
	G		Gypsums
	Gc		Gypsums in chaotic deposits
USE	**11**		Urban fabric
	12		Industrial, commercial and transport units
	13		Mine, dump and construction sites
	14		Artificial, non-agricultural vegetated areas
	21		Arable land
	22		Permanent crops
	23		Pastures
	24		Heterogeneous agricultural areas
	31		Forests
	32		Scrub and/or herbaceous vegetation associations
	33		Open spaces with little or no vegetation
	41		Inland wetlands
	51		Inland waters

survey began in 2005 and was further updated until 2018; a new field survey started in June 2019, but these new updates have not yet been completed by the Geological Survey of the Emilia-Romagna, which identifies three different landslide activity states, as active, inactive and quiescent. The latter is peculiar of larger landslides with intermittent activity, where the slow movements are alternating with long periods of quiescence and the return period can be more than a generation (https://ambiente.regione.emilia-romagna.it/en/geologia/geology/land-instabilities/le-caratteristiche-dei-fenomeni-franosi-in-emilia-romagna).

More in detail, 2567 landslides have been recognized in the Bidente basin, 1388 of which are active and 1179 are quiescent. Most of the active landslides represent the partial or total reactivation of large slope instabilities dated to the end of the LGM (Tellini and Chelli, 2003; Bertolini et al., 2004; Bertolini et al., 2017; https://ambiente.regione.emilia-romagna.it/it/geologia/geologia/dissesto-idrogeologico/le-caratteristiche-dei-fenomeni-franosi-in-emilia-romagna), while the new activation are less frequent.

The study area presents 1379 slides, 840 complex, and 348 flows (Fig. 2), with very few examples of falls\topples and unclassified cases that are not considered in the present work. Starting from the original polygon-based inventory, for each recognized phenomenon, the Landslide Identification Point (LIP), which corresponds to the highest point along the landslide crown, has been extracted. The recognition of the movement type following Cruden and Varnes (1996) was carried on in GIS environment, considering lithological and morphometric parameters as area, perimeter, and area-perimeter ratio, length, width, number of crowns for each landslide, slope, and circularity (https://ambiente.regione.emilia-romagna.it/it/geologia/geologia/dissesto-idrogeologico/le-caratteristiche-dei-fenomeni-franosi-in-emilia-romagna). The dataset here presented is available online at the following link: https://ambiente.regione.emilia-romagna.it/it/geologia/cartografia/webgis-banchedati/cartografia-dissesto-idrogeologico#consulta-dati-shp.

3. Material and methods

3.1. Diagnostic area, mapping units and geo-environmental predictors

According to previous applications (e.g., Rotigliano et al., 2011; Lombardo et al., 2015; Cama et al., 2015, 2017; Rotigliano et al., 2018, Martinello et al., 2023a,b,c, Mercurio et al., 2021), LIPs and 10 m-grid cells were assumed respectively as diagnostic landforms and mapping

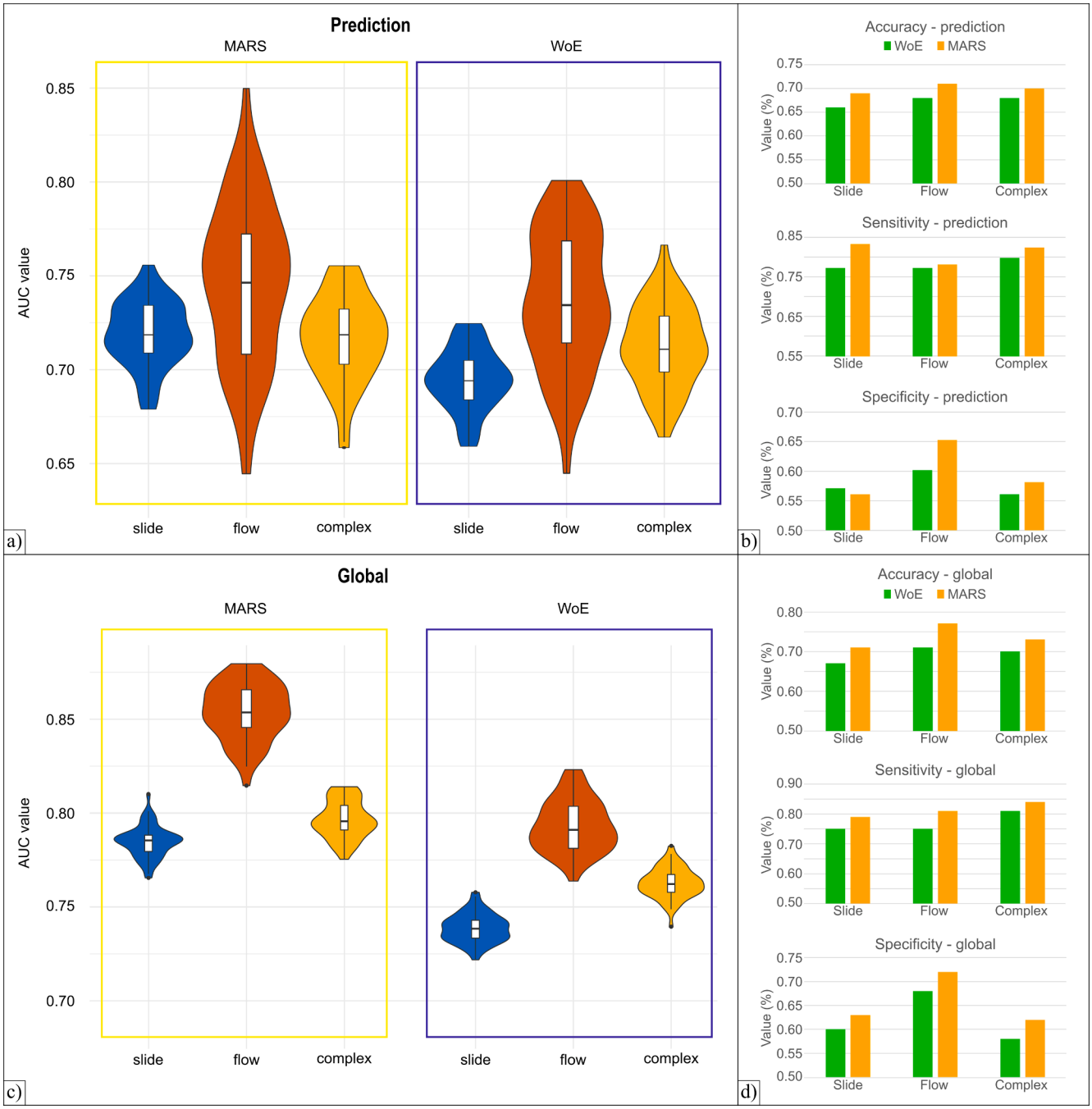

Fig. 3. Violin plots of AUC values obtained reiterating one-hundred prediction (a) and global (c) validations for slide, flow and complex landslide types. Corresponding bar plots of performance metrics computed in prediction (b) and global (d) validation schemes for slide, flow and complex landslide types. As the modelling procedures was based on positive/negative balanced subsets, FP and FN cases are complementary to sensitivity (true positive rate) and specificity (true negative rate), respectively.

units, suitable for expressing and capturing potentially unstable slope conditions.

As regards the controlling factors or covariates, a set of 10 geo-environmental variables was first set to express landslide occurrence controlling factors in the area, with a direct or proxy role (Costanzo et al., 2012; Martinello et al., 2022a,b). In particular: elevation (ELE), is here considered as a proxy for the spatial distribution of mean monthly/annual rainfall; plan (PLC) and profile (PRF) curvature, which describe the geometry of the slope along the horizontal and vertical planes respectively, express the geometry of the slopes and as such were considered as proxies for the convergence/divergence both of shallow gravitational stresses and surface runoff water (Ohlmacher, 2007); slope (SLO) controls the speed of the runoff water and the geometry of potential rupture surfaces (Martinello et al., 2022b); stream power index (SPI) expresses the intensity of surface water erosion (Martinello et al., 2022b); the topographic wetness index (TWI) describes the potential infiltration and is so considered as a proxy for the potential presence and thickness of a saturated soil horizon (Rotigliano et al., 2011; Martinello et al., 2022b); aspect (ASP) is considered a proxy for the seasonal wet/dry cycles of soils (Auslander et al., 2003) and strata attitude; landform classification (LCL) reflects the geomorphological setting of slopes; the lithotechnical outcropping unit (LITO) is considered as a proxy for the physical–mechanical properties of rocks (Martinello et al., 2022b); and land use (USE) potentially controls the hydrological and runoff water

SLIDE

Landslide susceptibility classes WoE	Landslide susceptibility classes MARS: low	moderate	high	very high	WoE
low	31%	8%	2%	0%	41%
moderate	5%	10%	6%	2%	23%
high	1%	6%	9%	7%	24%
very high	0%	1%	3%	8%	13%
MARS	37%	24%	20%	18%	

a)

FLOW

Landslide susceptibility classes WoE	Landslide susceptibility classes MARS: low	moderate	high	very high	WoE
low	36%	7%	2%	0%	44%
moderate	6%	9%	7%	1%	23%
high	2%	5%	10%	2%	19%
very high	1%	2%	7%	4%	13%
MARS	45%	22%	26%	7%	

b)

COMPLEX

Landslide susceptibility classes WoE	Landslide susceptibility classes MARS: low	moderate	high	very high	WoE
low	35%	7%	2%	0%	44%
moderate	3%	10%	9%	4%	25%
high	1%	2%	6%	10%	20%
very high	0%	0%	1%	9%	11%
MARS	39%	20%	18%	24%	

c)

Fig. 4. Comparison of the different susceptibility classes derived from the application of MARS and WoE methods, related to a) slide, b) flow, c) complex landslide types. Main cut-offs are reported with orange (for MARS) and light green (for WoE) lines. Values in the light blue box represent the critical two classes switch while with red write fill are reported the critical one class cases.

erosion induced disturbances (Martinello et al., 2022b).

All the variables derived from Digital Elevation Model (DEM) were calculated by using tools of SAGA GIS (Conrad et al., 2015). ASP, LCL, LITO, and USE were employed as categorical variables (Table 1) while, due to the specific requirements of the statistical methods used in this research, the DEM-derived variables, which were used as continuous by MARS, were re-classified and categorized for WoE analysis. In particular, natural breaks of ELE, SPI, and TWI were employed to discriminate five categorical classes of these predictors; for SLO, ten classes were defined according to the expected different influence in determining slope instability; lastly, for PLC and PRF, five classes of each variable were defined using a symmetrical classification around 0 (flat) and defining other two classes both for convex (values < 0) and concave (values > 0) settings. The categorical classes of the DEM-derived predictors and the relative numerical interval are reported in Table 1.

For each pixel, the predictors information (as continuous or categorical classes) was first assigned. Then, by overlapping the LIPs with the grid cells, each pixel was also classified as stable or unstable with respect to each typology of landslide analysed, based on the presence/absence of at least one LIP.

3.2. Statistical methods

The goal of the research was carried out through the comparative application of *Weight of Evidence* (WoE) and *Multivariate Adaptive Regression Splines* (MARS) statistical methods aimed at assessing landslide susceptibility in the Bidente River basin. The analysed landslides included slide, flow and complex types.

3.2.1. Weight of Evidence (WoE)

Weight of Evidence (WoE) is a statistical method based on the Bayes' theorem. The details are reported in Bonham-Carter (1989). By overlaying landslides with each causal factor, the statistical incidence can be measured between them. A pair of weights, W^+ and W^-, for each class of each causal factor is then computed as follows:

$$W^+ = ln\left(\frac{\frac{A_1}{A_1+A_2}}{\frac{A_3}{A_3+A_4}}\right) \tag{1}$$

and

$$W^- = ln\left(\frac{\frac{A_2}{A_1+A_2}}{\frac{A_4}{A_3+A_4}}\right) \tag{2}$$

where A_1 is the number of the LIPs in a given factor class, A_2 is the number of LIPs not present in the given factor class, A_3 is the number of the cells in the given factor class in which no LIPs are present, and A_4 is the number of cells in which neither LIPs nor the given factor class is present. The difference between W^+ and W^- is called contrast C. The overall landslide susceptibility LS for each cell can be computed by summing the contrast values of each causal factor:

$$LS = \sum_{i=1}^{n} C_{i,j} \tag{3}$$

where $C_{i,j}$ is the contrast value for the class j of factor i and n is the total number of factors.

Differently from what is typically observed, before proceeding to the validation of the WoE model, in order to constrain the final score into a 0–1 range, a score normalization was finally applied by adding the minimum (to shift the values in the positive range) and dividing by the maximum.

For this research, WoE analysis was performed by exploiting RStudio software.

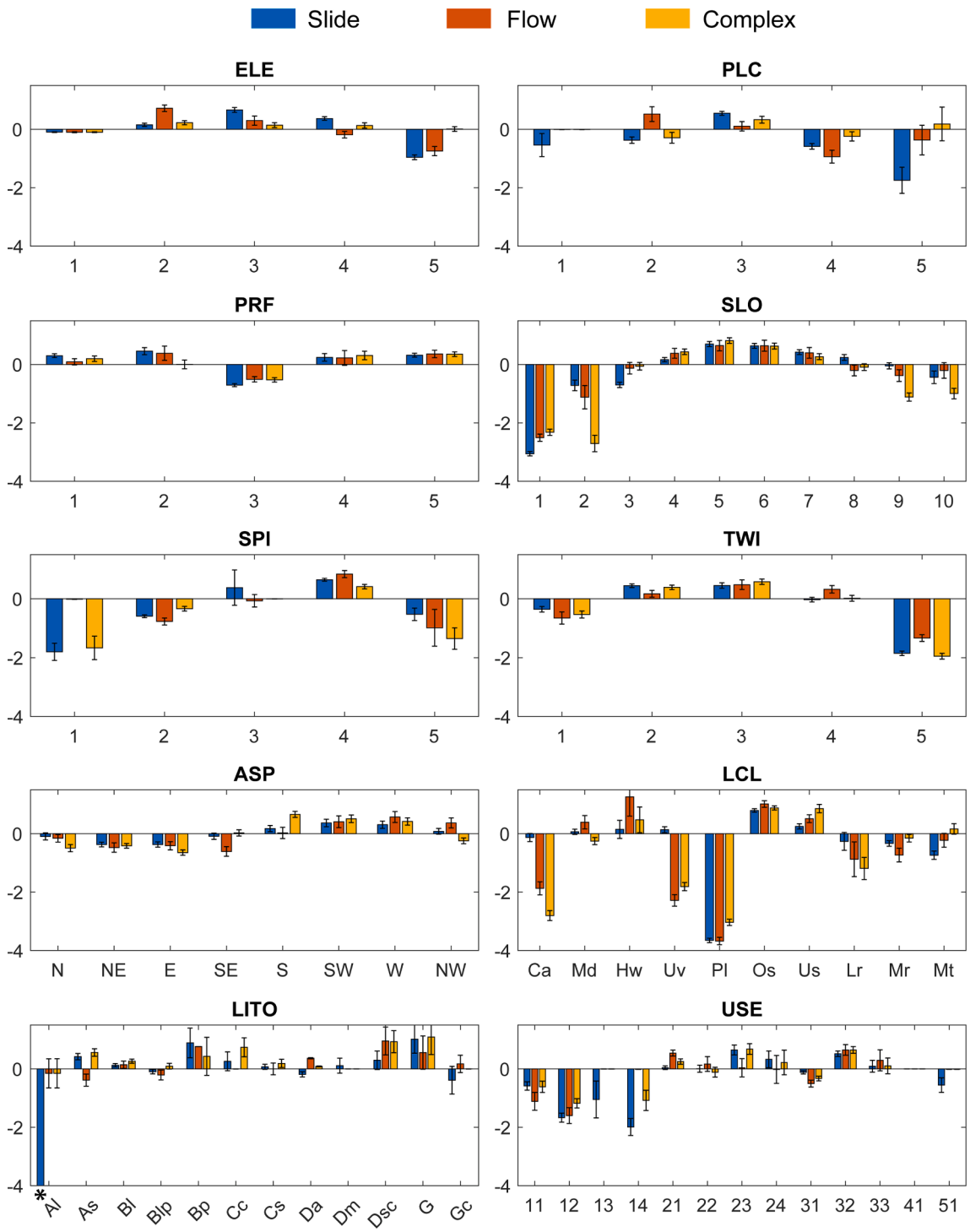

Fig. 5. Bar plots showing mean contrast and standard deviation of each class of the predisposing factors related to slide, flow and complex types. Covariate classes values are explained in Table 1. *Contrast value outlier.

3.2.2. *Multivariate adaptive regression splines (MARS)*

The *Multivariate Adaptive Regression Splines* (MARS) is a non-parametric regression method that exploits the partitioning of each independent variable into hinge functions to increase the fit based on the maximum likelihood of the logistic regression method (Friedman, 1991), according to the relation:

$$y = f(x) = \alpha + \sum_{i=1}^{n} \beta_i h_i(x) \quad (4)$$

where y is the dependent variable (the outcome) predicted by the function $f(x)$, α is the model intercept, β_i are the coefficients of the h_i basis functions and n is the number of basis functions. MARS analysis was here performed by exploiting the "earth" package (Milborrow, 2021) of RStudio software. The default setting of the "earth" package (please refer to the notes on the "earth" package) was used, limiting the MARS terms to a range of 20–200 and building a simple additive model (no interaction terms).

In recent years, MARS has been largely adopted for landslide susceptibility modelling (e.g., Vorpahl et al., 2012; Conoscenti et al., 2015; Vargas-Cuervo et al., 2019; Martinello et al., 2023a, b; Mercurio et al.,

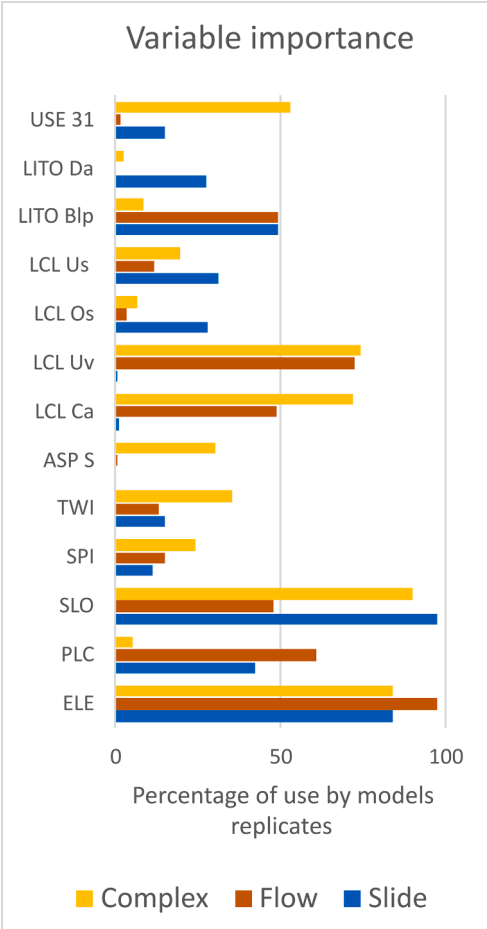

Fig. 6. Bar plots showing the variable importance for MARS models calculated as the percentage of variable use by each replicated set. Covariate classes values are explained in Table 1.

2023).

3.3. Validation and model building strategies

Both WoE and MARS modelling procedures are based on a presence–absence approach. In fact, to correctly evaluate equations (1) and (2), for the WoE method a balanced data frame is necessary; at the same time, the MARS method defines positive relationships between (intervals of) variables and stable/unstable cases. Therefore, the same number of negative and positive cases had to be randomly extracted. To test the resolution, precision, and robustness of the models (i.e., the independence of the results from the choice of the selected cases), one-hundred random extractions of the balanced datasets were performed (Martinello et al., 2023c; Mercurio et al., 2021; Rotigliano et al., 2019). Each of the one-hundred balanced archives was then randomly split to obtain a sub-set exploited for the calibration (75 %) of the model and a sub-set for its validation (25 %). According to Chung and Fabbri (2003), the prediction skill performance was first evaluated, by testing the recall capacity of the validation subset for the model calibrated exploiting the complementary 75 %. Then, a global performance was evaluated by applying the calibrated model to the whole balanced archive, configuring a mixed test (success for 75 % + prediction for 25 %). This procedure was implemented for each investigated landslide typology.

The accuracy of the models was evaluated by the AUC value (Area Under Curve) in the ROC (Receiver Operating Characteristics; Fawcett, 2006; Goodenough et al., 1974; Lasko et al., 2005) plots, referring to Hosmer and Lemeshow (2000) thresholds. Moreover, Youden index optimised cut-offs (Youden, 1950) were obtained from each ROC plot, to prepare cut-off dependent confusion matrices and evaluate binarized True Positive (TP), True Negative (TN), False Positive (FP) and False Negative (FN) cases. By applying a nested Youden index-based score reclassification (Martinello et al., 2021), four landslide susceptibility levels (low, moderate, high, and very high by employing the low, medium, and high Youden index cut-off, respectively) were discriminated. It is worth noting that each model generated a specific pixel score assignment, resulting in specific ROC-plot, cut-offs, and confusion matrices.

To investigate the inner structure of the models, the replicates were also exploited for evaluating the frequency distribution of the contrast of each variable, for WoE models, as well as the variables' importance, for MARS models. In the case of WoE the magnitude of the contrasts which the classes of the various factors get in the modelling is directly taken as an importance index. Differently, for MARS, the percentage of use of each variable by the replicates, which was calculated by using the "varImp" function of the Caret (Kuhn, 2016) R-package, was considered. However, an a posteriori factor analysis was also carried out, by exploring the actual correlation between predicted susceptibility score and covariates values.

4. Results

4.1. Model performance

The AUC values of models' replicates which were obtained for each analysed landslide type are shown by violin plots in Fig. 3, both for prediction (Fig. 3a) and global (Fig. 3c) validations.

Largely satisfactory accuracy values were achieved for WoE prediction (AUC = 0.69, 0.73, and 0.71 for slide, flow, and complex type, respectively) and global (AUC = 0.74, 0.78, and 0.76 for slide, flow, and complex type, respectively) validation. Higher performances resulted for MARS prediction (0.72, 0.75, and 0.72 for slide, flow, and complex type, respectively) and global (0.78, 0.85, and 0.79 for slide, flow, and complex type, respectively) ROC plots. Besides, for both methods a larger variability of the AUC values for prediction skill were observed through the one-hundred replicates, especially for the flow-type models.

As regards the binarized accuracy evaluation (Fig. 3b and d), similar behaviours arose for the prediction validation: sensitivity values are good (>0.77) for WoE and even excellent for MARS (over 0.8 for slide and complex analysis). Conversely, the sensitivity of all types of models suffers for a widely marked FPs production and, consequently, a general lower accuracy.

In the global validation, the sensitivity shows the highest value for the complex-type analysis, both using MARS and WoE methods (0.84 and 0.81, respectively). Sensitivity values, ranging between 0.75 and 0.81 attests for a good skill of the models in detecting positive cases. On the other hand, specificity reaches satisfactory values for MARS (0.71) and for WoE (0.68) only for the flow-type model: for all the other landslide types, very low (around 0.55) sensitivity values were achieved. Obviously, this reveals a high number of FPs, especially produced for slide and complex (~40 %) landslide models. Due to the low performance in detecting TN cases, balanced accuracy produced good values employing MARS method (0.71, 0.77 and 0.73 for slide, flow and complex, respectively) and lower values for WoE (0.67, 0.71 and 0.7 for slide, flow and complex, respectively).

Fig. 4 shows the accuracy of the landslide susceptibility models for the three types of landslides analysed using MARS and WoE methods, arranged in four-classes confusion matrices (low, moderate, high, very high). The cut-off thresholds separating consecutive classes have been obtained through a nested application of the Youden Index criterion cut-off. The last column/row of each table, named WoE/MARS, reports the percentage of cases included in a specific susceptibility class by the two methods. Similar percentages of cases were classified as low, both for MARS (37 %, 45 % and 39 % for slide, flow, and complex types,

Table 2
Values associated to the decile classes for each continuous variable.

ELEV		PLC		PRF	
Class	*m (a.s.l.)*	*Class*	*rad/m*	*Class*	*rad/m*
1	0–26	1	<-1.04	1	<-0.0059
2	26–116	2	-1.04–-0.62	2	-0.0059–-0.0033
3	116–205	3	-0.62–-0.20	3	-0.0033–-0.0016
4	205–295	4	-0.20–0.20	4	-0.0016–-0.0008
5	205–404	5	0.2–0.62	5	-0.0008–0.0008
6	404–507	6	0.62–1.04	6	0.0008–0.0009
7	507–609	7	1.04–1.45	7	0.0009–0.0026
8	609–732	8	1.45–2.29	8	0.0026–0.0043
9	732–886	9	2.29–4.79	9	0.0043–0.0069
10	>1650	10	>4.79	10	>0.0069
SLO		**SPI**		**TWI**	
Class	*degree*	*Class*	*kg m^2/s^{-3}*	*Class*	*m*
1	<0.3	1	<3882	1	<5.8
2	0.3–5.9	2	3882–7764	2	5.8–6.3
3	5.9–10	3	7764–11647	3	6.3–6.8
4	10–14	4	11647–15529	4	6.8–7.3
5	14–18.1	5	15529–23294	5	7.3–7.8
6	18.1–22.6	6	23294–34941	6	7.8–8.4
7	22.6–27.1	7	34941–50470	7	8.4–9.2
8	27.1–31.5	8	50470–81529	8	9.2–10.4
9	31.5–36.8	9	81529–993885	9	10.4–11.9
10	>36.8	10	>993885	10	>11.9

respectively) and WoE (41 %, 44 % and 44 % for slide, flow, and complex types, respectively). At the same time, similar percentages for all the landslide types, ranging between 18 % and 26 %, characterized the moderate and high classes. Generally, the very high class is the less populated with a percentage ranging between 7 % and 13 %, except for those defined by MARS for slide (18 %) and complex (24 %).

A combined analysis permitted the evaluation of the percentage of congruent (reported in the diagonal of each table) and un-congruent cases (all the other boxes) classified by the two statistical methods. The analysis showed a general congruence of the two methods: 58 %, 59 % and 60 % for slide, flow, and complex type, respectively. Only a few cases are characterized by a critical switch of classes, corresponding to a shift across the main cut-off. For slide landslides, 18 % of critical cases was observed, with 12 % of cases corresponding to one-class switch. Similarly, for flow landslides, 20 % of critical cases was observed, 12 % of which corresponding to a one-class switch. Finally, for complex landslides, 18 % of critical cases were generated, with 12 % limited to a one-class switch, with 15 % of cases classified as high or very high (11 % and 4 %, respectively) by MARS, but estimated as low (2 %) or moderate (13 %) by WoE and 3 % of cases classified as high by WoE, but low (1 %) or moderate (2 %) by MARS. This kind of asymmetry was not recorded for flow and slide.

4.2. Importance of variables

4.2.1. Contrast values of predictor classes for WoE

The variable importance for WoE models can be understood by examining the bar plots in Fig. 5. These plots show the mean contrast and standard deviation through the replicates for each class of predisposing factors across all landslide types.

Regarding ELE, the highest positive incidence for slides occurs from 371 to 500 m a.s.l. (“3”), while for flows and complex landslides, it is from 27 to 71 m a.s.l. (“2”).

PLC shows negative incidence for slides in the very convex, convex, concave, and very concave classes (“1”, “2”, “4”, “5”), but positive incidence in the flat class (“3”). For flows, positive contrasts are observed in the convex and flat classes (“2”, “3”), and negative contrasts in the concave and very concave classes (“4”, “5”). Complex landslides show a negative impact in the convex and concave classes (“2”, “4”), but a positive impact in the flat and very concave classes (“3”, “5”).

PRF consistently shows positive contrasts for all types of landslides, except for the negative incidence in the flat class (“3”).

In terms of SLO, there is a general agreement among landslide types. Negative contrasts are observed up to 10° (“3”), beyond which the incidence becomes positive up to 45° (“9”), with the maximum values occurring between 20° and 25° (“5”).

The SPI factor also exhibits consistency among landslide types. The greatest positive impact is found from 184.8 and 20605.7 kg $m^2 s^{-3}$ (“3”, “4”), while the other classes show negative values.

The TWI factor shows positive values from 5.73 and 8.29 m (“2”, “3”), while negative values are observed for values greater than 10.42 m (“5”) and lower than 5.73 m (“1”).

ASP has a negative or zero impact for azimuths from N to SE and a positive impact for azimuths from S to NW for all types of landslides. However, complex landslides on NW azimuths show a negative contrast.

LCL generally agrees with the incidence of classes among different landslide types, except for Midslope drainages (“Md”) where only flows show positive values, U-shaped valleys (“Uv”) where slides have slightly positive values compared to the strongly negative values of other types, and Mountain tops (“Mt”) where only complex landslides show positive values.

LITO exhibits wide variability in contrasts among landslide types. Positive impacts on slides are observed in classes such as sandstone/pelitic alternations with S/P < 0.3 (“Bp”), stratified massive rocks (“As”), gypsums (“G”), tectonized clays and argillites (“Dsc”), and clast-supported conglomerates (“Cc”). Similar positive impacts are seen on flows and complex landslides with variations in specific classes. Negative values are recorded in alluvial plain deposits (“Al”) for all types, particularly for slides, and in other specific classes.

Finally, for USE, there is concordance in the incidence of classes among landslide types. Positive values are observed in classes such as shrub and/or herbaceous vegetation associations (“32”), pastures (“23”), arable land (“21”), and heterogeneous agricultural areas (“24”). Negative values are found in classes such as industrial, commercial, and transport units (“12”), urban fabric (“11”), mine, dump, and construction sites (“13”), artificial, non-agricultural vegetated areas (“14”), and forest (“31”).

4.2.2. Predictor importance for MARS

In Fig. 6 the variables’ importance for the MARS models, calculated as the percentage of variable use by each replicated set, is shown. SLO and ELE are the most frequently used variables, but if the latter obtain high values for all the typologies (84 %, 97 % and 84 % for slide, flow, and complex movements, respectively), the former is heavily used only by slide (97 %) and complex (90 %).

Setting a threshold of 30 % of recall, it is possible to discriminate between variables employed only for two out of three typologies and others whose importance resulted as significant only for one type. Among the classes of LCL, large use of U-shaped valleys (“Uv”) and Canyons (“Ca”) classes were selected for flow (72 % and 49 %, respectively) and complex (74 % and 72, respectively) models. Besides, for slide and flow models PLC (42 % and 61 %, respectively) and “Blp” (sandstone/pelitic alternations with 0.3 < S/P < 3) of LITO (49 % for both) were employed.

S class of ASP, forest class (“31”) of USE, and TWI were used only for complex-type models (30 %, 53 % and 35 %, respectively). Finally, the upper slopes (“Us”) class of LCL is used by 31 % of slide models’ replicates.

4.3. Analysis of the correlation between landslide susceptibility score and predictors

According to the aim of this research, a deeper analysis of the correlation between the susceptibility score and the variability of the predictors was carried out. In particular, to more directly compare the role that the two modelling methods assigned to each covariate, the

Fig. 7. Relationship between the classes of variables and δ-score of slide landslides obtained by MARS and WoE models. a - f) Comparison between the deciles of continuous variables and the δ-score; g-j) relationship between the classes of categorical variables and the δ-score.

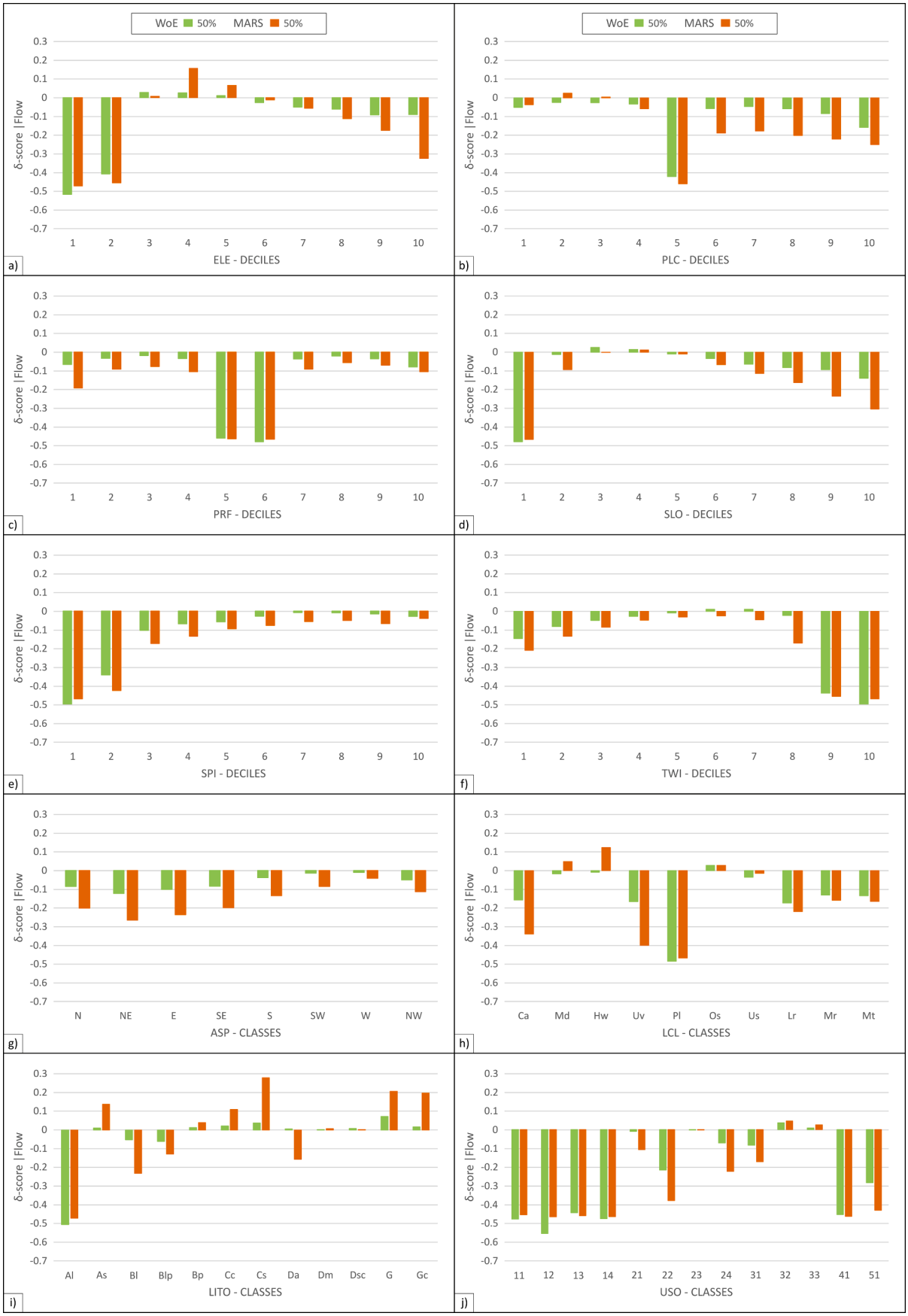

Fig. 8. Relationship between the classes of variables and δ-score of flow landslides obtained by MARS and WoE models. a - f) Comparison between the deciles of continuous variables and the δ-score; g-j) relationship between the classes of categorical variables and the δ-score.

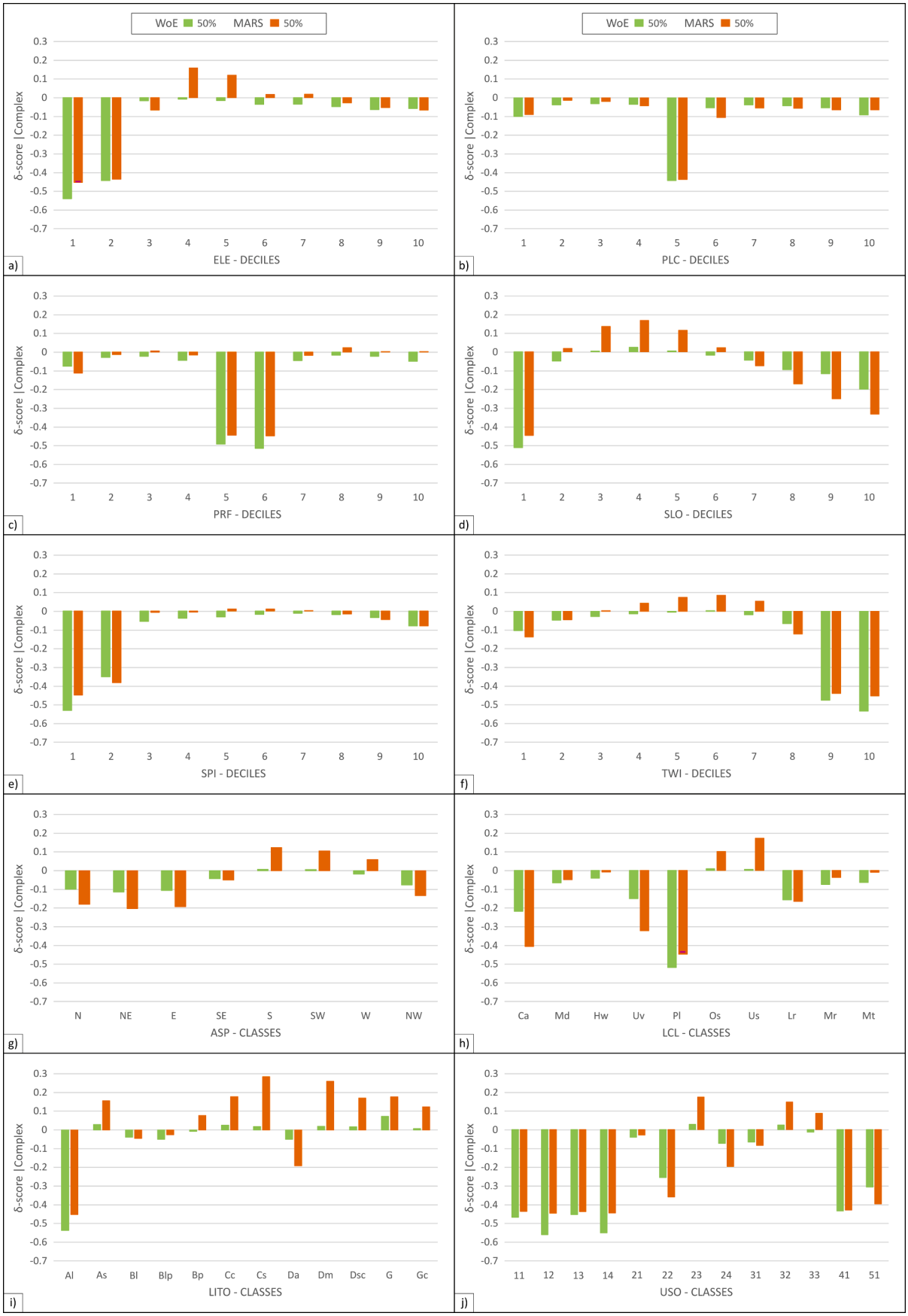

Fig. 9. Relationship between the classes of variables and δ-score of complex landslides obtained by MARS and WoE models. a - f) Comparison between the deciles of continuous variables and the δ-score; g-j) relationship between the classes of categorical variables and the δ-score.

difference between the susceptibility score and the specific cut-off values (δ-score) were plotted for each factor class, for categorial, or deciles class, for continuous variables (the values corresponding to each decile class are reported in Table 2). In order to simplify the graphs, the δ-score were reported (Figs. 7, 8, and 9) by bar. In particular, the bar amplitude reflects the potential correlation between each class and the associated score, with large bars strongly marking positive or negative status prediction.

In general, very similar factor trends emerged between the two statistical methods with an almost systematic coherence of unstable and stable cases prediction, corresponding to positive or negative δ-score, respectively. Besides, with some specific exception, similar trends were recognized for the three landslide typologies.

Strong negative coherent correlations arose for one or more class of all the factors, whilst less marked and coherent (limited to one or two classes for factor) positive correlations resulted, especially for the DEM-derived variables. In particular, for the latter, marked negative correlations were observed for all the three typologies at: values lower than 116 m a.s.l. (class "1" and "2" of ELE); from 0.2 to 0.62 rad/m (class "5" of PLC); from −0.0008 and 0.0009 rad/m (class "5" and "6" of PRF); values lower than 0.3° (class "1" of SLO); values lower than 7764 kg m^2/s (class "1" and "2" of SPI); values greater than 10.4 m (class "9" and "10" of TWI); plains ("Pl") LCL class. ASP shows only minor negative correlation for NE facing pixels.

High SLO and TWI values are associated to stable predicted status for the three typologies, together with a smoothed decreasing negative δ–score for SPI. Negative δ–scores are marked for Local ridges ("Lr"), Midslope ridges ("Mr") and Mountain tops ("Mt") LCL classes, for Canyons ("Ca") and U-shaped valley ("Uv") classes, limited to flow and complex landslides, and Headwaters ("Hw") class, for slides. On the contrary, positive δ–scores were observed for Open slopes ("Os") and Upper slopes ("Us"), for complex landslides, Midslope drainage ("Md") and Headwaters ("Hw"), for flows, and Open slopes ("Os"), for slides.

As regards the categorial variable, much more discriminated results were observed. In facts, for all the three considered typologies, strong or smoothed negative correlations arose for the alluvial plain deposits ("Al") class and the consolidated clays ("Da"), sandstone/pelitic alternations with S/P > 3 ("Bl") and sandstone/pelitic alternations with 0.3 < S/P ("Blp") LITO classes, respectively. At the same time, strong positive correlations were observed for weakly cemented sands ("Cs"), for complex and flows, and marls ("Dm") and tectonized clays and argillites ("Dsc"), for complex. Smoothed positive correlation for any typology marked the classes stratified massive rocks ("As"), sandstone/pelitic alternations with S/P < 0.3 ("Bp"), clast-supported conglomerates ("Cc"), gypsums ("G") and gypsums in chaotic deposits ("Gs"). Regarding the USE, negative δ-scores were observed at the classes: urban fabric ("11"), industrial, commercial and transport units ("12"), mine, dump and construction sites ("13"), artificial, non-agricultural vegetated areas ("14"), permanent crops ("22"), inland wetlands ("41"), inland waters ("51"), for the three typologies, whilst the classes pastures ("23"), scrub and/or herbaceous vegetation associations ("32") e open spaces with little or no vegetation ("33") featured positive values (smoothed for flow).

5. Discussion

According to the results, MARS and WoE allowed to obtain performing susceptibility models in the Bidente river basin, attested by good or excellent ROC_AUC, with high performance indexes for MARS, both in the cut-off independent and dependent domains. In particular, for all the three typologies, MARS systematically performs with a slightly higher accuracy both in negative and positive cases prediction. However, when passing to a binarized analysis, such slight differences do not produce any marked effects. In facts, a very limited number of critical mismatching cases was observed, which configure under versus over cut-off estimation of the predicted status between the two methods. Among these critical mismatching cases, the largest incidence is due to only one-class shift. The critical cases are symmetrically distributed with respect to the two methods for slides and flow landslides, whilst for complex landslides largely prevails the cases (15 % against 3 %) where MARS and WoE predict an over against an under-cut-off status, respectively.

A strong general congruence also arose for the set of explanatory variables which MARS and WoE exploited to fit the positive/negative spatial distribution. In facts, among both the categorial and numerical predictors, the two methods mainly rely their prediction on the same lithologic, soil use, topographic and morphologic variables. This has been made clear by analysing the pattern of the score through the classes of each factor, systematically obtaining very similar trends.

Regarding the importance of the factors in discriminating landslide types, SLO and TWI factors appear to be among the most distinctive. Indeed, although slope inclinations between 10° and 14° (class "4") are predisposing for all three types, flow types begin to be predisposed by slopes from 5.9° (class "3"), as do complex failures. The latter, however, extend up to slopes of 22.6° (class "6"), which are also reached by the slides. The inclusiveness of the complex typology of both other two typologies shows how this typological attribution is used as an alternative to a more specific characterization and is therefore inclusive of both kinematisms. Specular is the trend of the TWI factor for which the complex typology similarly includes both the trend of flows (6.8 to 8.4 - classes "4", "5", and "6") and slides (7.8 to 9.2 - classes "6", and "7").

Among the categorical factors, the most important is the LCL, which mainly allows the flow types to be distinguished from the other kinematisms. In fact, these are more prone in the Headwaters ("Hw") and Midslope drainage "Md", while the complex landslides in the Upper slopes ("Us") and Open slopes ("Os") and the slides only in the Open slopes ("Os"). LITO also proved to be a discriminating factor. Specifically, although an increase in the percentage of pelitic component in the alternations ("Bl" to "Bp") increases the susceptibility of all kinematics, complex and slide are the most affected. Weakly-cemented sands ("Cs") and clast-supported conglomerates ("Cc") predispose the flow and complex types the most, while slides generated only from clast-supported conglomerates ("Cc"). Finally, marls ("Dm") and tectonised clays and argillites ("Dsc") characterise the complexes more. The ASP factor is distinctive for complex landslides, identifying S, SW, and W exposed slopes as predisposing unlike the other kinematisms.

On the base of the set of predictors which emerged as controlling factors, geomorphologically adequate models arose for the three landslide typologies, with LITO and LCL classes delimiting the landslide domains and topographic attributes (steepness, curvatures, SPI, and TWI) modulating the score inside.

6. Conclusions

In spite of the different approaches MARS and WoE rely on, river basinvery similar results have been obtained in terms of prediction skill of the derived susceptibility models in the Bidente river vasint . A difference, attesting a more ability of MARS in fitting the observed data actually emerged. Nonetheless, this result could depend on the general state of activity of the slopes of the Bidente catchments. In fact, the more potential instable sites have been triggered and produce TP cases, the more multivariate regression and bivariate conditional analysis-based methods will furnish similar outputs. At the same time, different driven landslide scenarios could stress the models in different ways, with a different response in terms of prediction skill. In particular, score differences which actually do not produce any change in the binary predicted status, could take importance in case of a cut-off variation.

The comparison between conditional analysis and regression-based methods, is out of doubts a very important issue considering the wide adoption of such approaches in landslide susceptibility modelling studies. Authors are aware that further tests must be carried out to include a representative enough case studies set. At the same time, a

reference for designing methods (normalized score and optimized cut-off) and tools (analysis of critical cases and variables' congruence) to quantitatively compare the results obtained by the two approaches is here proposed.

As regards the general topic of this research, investigating binarized susceptibility values inside each factor class seems to be suitable for giving any user a tool for applying geomorphological soundness criteria in assessing that model adequacy which should be a mandatory component of any model validation protocol.

CRediT authorship contribution statement

Chiara Martinello: Conceptualization, Methodology, Software, Formal analysis, Investigation, Visualization, Writing – original draft, Writing – review & editing. **Michele Delchiaro:** Conceptualization, Methodology, Software, Formal analysis, Investigation, Visualization, Writing – original draft, Writing – review & editing. **Giulia Iacobucci:** Visualization, Writing – original draft, Writing – review & editing. **Chiara Cappadonia:** Supervision, Writing – review & editing. **Edoardo Rotigliano:** Conceptualization, Methodology, Writing – review & editing, Supervision, Project administration. **Daniela Piacentini:** Conceptualization, Methodology, Writing – review & editing, Supervision, Project administration.

Declaration of competing interest

The authors declare that they have no known competing financial interests or personal relationships that could have appeared to influence the work reported in this paper.

Data availability

Data will be made available on request.

Acknowledgements

This study was carried out within the RETURN Extended Partnership and received funding from the European Union Next-GenerationEU (National Recovery and Resilience Plan – NRRP, Mission 4, Component 2, Investment 1.3 – D.D. 1243 2/8/2022, PE0000005). At the same time, this research is also the result of a collaboration between different universities (University of Palermo and Sapienza University of Rome) in the frame of the workgroup of AIGeO (Italian Association of Physical Geography and Geomorphology) "Environmental and Applied Geomorphology".

Appendix A. Supplementary material

Supplementary data to this article can be found online at https://doi.org/10.1016/j.catena.2024.107835.

References

Al-Najjar, H.A.H., Pradhan, B., Kalantar, B., Sameen, M.I., Santosh, M., Alamri, A., 2021. (2021. Landslide Susceptibility Modeling: An Integrated Novel Method Based on Machine Learning Feature Transformation. Remote Sens 13, 3281. https://doi.org/10.3390/rs13163281.

Antolini, G., Auteri, L., Pavan, V., Tomei, F., Tomozeiu, R., Marletto, V., 2015. A daily high-resolution gridded climatic data set for Emilia-Romagna, Italy, during 1961–2010. Int. J. Climatol. 36 (4), 1970–1986. https://doi.org/10.1002/joc.4473.

Antolini, G., Pavan, V., Tomozeiu, R., Marletto, V., 2017. Atlante climatico dell'Emilia-Romagna 1961-2015. https://www.arpae.it/it/temi-ambientali/clima/rapporti-e-documenti/atlante-climatico.

Atkinson, P.M., Massari, R., 1998. Generalized linear modelling of susceptibility to landsliding in the Central Apennines. Geomorphology 130 (1–2), 55–64. https://doi.org/10.1016/j.geomorph.2011.02.001.

Auslander, M., Nevo, E., Inbar, M., 2003. The effects of slope orientation on plant growth, developmental instability and susceptibility to herbivores. J. Arid Environ. 55, 405–416. https://doi.org/10.1016/S0140-1963(02)00281-1.

Bartolini, C., 2003. When did the Northern Apennine become a mountain chain? Quat. Int. 101–102, 75–80. https://doi.org/10.1016/S1040-6182(02)00090-3.

Bertolini, G., Casagli, N., Ermini, N., Malaguti, C., 2004. Radiocarbon Data on Lateglacial and Holocene Landslides in the Northern Apennines. Nat. Hazards 32, 645–662. https://doi.org/10.1023/B:NHAZ.0000024896.34933.63.

Bertolini, G., Guida, M., Pizziolo, M., 2005. Landslides in Emilia-Romagna region (Italy): strategies for hazard assessment and risk management. Landslides 2, 302–313. https://doi.org/10.1007/s10346-005-0020-1.

Bertolini, G., Corsini, A., Tellini, C., 2017. Fingerprints of Large-Scale Landslides in the Landscape of the Emilia Apennines. In: Soldati, M., Marchetti, M. (Eds.), Landscapes and Landforms of Italy. World Geomorphological Landscapes. Springer, Cham. https://doi.org/10.1007/978-3-319-26194-2_18.

Bonham-Carter, G.F., 1989. Weights of evidence modelling: a new approach to mapping mineral potential. Statist. Appl. Earth Sci. 171–183.

Brabb, E.E., 1984. Innovative approaches to landslide hazard and risk mapping. International landslide symposium proceedings, Toronto, Canada 1, 17–22.

Bufalini, M., Materazzi, M., De Amicis, M., Pambianchi, G., 2021. From traditional to modern 'full coverage' geomorphological mapping: a study case in the Chienti river basin (Marche region, central Italy). J. Maps. https://doi.org/10.1080/17445647.2021.1904020.

Cama, M., Lombardo, L., Conoscenti, C., Agnesi, V., Rotigliano, E., 2015. Predicting Storm-Triggered Debris Flow Events: Application to the 2009 Ionian Peloritan Disaster (Sicily, Italy). Nat. Hazards Earth Syst. Sci. 15, 1785–1806. https://doi.org/10.5194/nhess-15-1785-2015.

Cama, M., Lombardo, L., Conoscenti, C., Rotigliano, E., 2017. Improving Transferability Strategies for Debris Flow Sus-ceptibility AssessmentApplication to the Saponara and Itala Catchments (Messina, Italy). Geomorphology 288, 52–65. https://doi.org/10.1016/j.geomorph.2017.03.025.

Carminati, E., Doglioni, C., 2012. Alps vs. Apennines: The paradigm of a tectonically asymmetric Earth. Earth Sci. Rev. 112 (1–2), 67–96. https://doi.org/10.1016/j.earscirev.2012.02.004.

Carrara, A., 1983. Multivariate models for landslide hazard evaluation. Journal of the International Association for Mathematical Geology 15, 403–426. https://doi.org/10.1007/BF01031290.

Chacón, J., Irigaray, C., Fernández, T., El Hamdouni, R., 2006. Engineering geology maps: landslides and geographical information systems. Bulletin of Engineering Geology and the Environment 65, 341–411. https://doi.org/10.1007/s10064-006-0064-z.

Chen, W., Peng, J., Hong, H., Shahabi, H., Pradhan, B., Liu, J., Duan, Z., 2018. Landslide susceptibility modelling using GIS-based machine learning techniques for Chongren County, Jiangxi Province, China. Sci. Total Environ. 626, 1121–1135. https://doi.org/10.1016/j.scitotenv.2018.01.124.

Chung, C. J. F., & Fabbri, A. G. (2003). Validation of spatial prediction models for landslide hazard mapping. *Natural Hazards*, *30*, 451-472. https://doi.org/10.1023/B:NHAZ.0000007172.62651.2b.

Conoscenti, C., Ciaccio, M., Caraballo-Arias, N.A., Gómez-Gutiérrez, Á., Rotigliano, E., Agnesi, V., 2015. Assessment of susceptibility to earth-flow landslide using logistic regression and multivariate adaptive regression splines: a case of the Belice River basin (western Sicily, Italy). Geomorphology 242, 49–64. https://doi.org/10.1016/j.geomorph.2014.09.020.

Conrad, O., Bechtel, B., Bock, M., Dietrich, H., Fischer, E., Gerlitz, L., Wehberg, J., Wichmann, V., Böhner, J., 2015. System for Automated Geoscientific Analyses (SAGA) v. 2.1.4. Geosci. Model Dev. 8, 1991–2007. https://doi.org/10.5194/gmd-8-1991-2015.

Conti, P., Cornamusini, G., Carmignani, L., 2020. An outline of the geology of the Northern Apennines (Italy), with geological map at 1:250,000 scale. Ital. J. Geosci. 139 (f2), 149–194. https://doi.org/10.3301/IJG.2019.25.

Costanzo, D., Rotigliano, E., Irigaray, C., Jiménez-Perálvarez, J.D., Chacón, J., 2012. Factors Selection in Landslide Sus-ceptibility Modelling on Large Scale Following the Gis Matrix Method: Application to the River Beiro Basin (Spain). Nat. Hazards Earth Syst. Sci. 12, 327–340. https://doi.org/10.5194/nhess-12-327-2012.

Costanzo, D., Chacón, J., Conoscenti, C., Irigaray, C., Rotigliano, E., 2014. Forward Logistic Regression for Earth-Flow Landslide Susceptibility Assessment in the Platani River Basin (Southern Sicily, Italy). Landslides 11, 639–653. https://doi.org/10.1007/s10346-013-0415-3.

Cruden, D.M., Varnes, D.J., 1996. Landslide types and processes. In: Turner, A.K., Shuster, R.L. (Eds.), Landslides: Investigation and Mitigation. Transportation Research Board, Spec Rep 247, pp 36–75.

Delchiaro, M., Rouhi, J., Valiante, M., Della Seta, M., Esposito, C., Martino, S., 2021. Bivariate landslide susceptibility analysis in the Lorestan Arc (Zagros Mountains, Iran). Italian J. Eng. Geol. Environ. 53–66. https://doi.org/10.4408/IJEGE.2021-01.S-05.

Delchiaro, M., Della Seta, M., Martino, S., Nozaem, R., Moumeni, M., 2023. Tectonic deformation and landscape evolution inducing mass rock creep driven landslides: The Loumar case-study (Zagros Fold and Thrust Belt, Iran). Tectonophysics 846, 229655. https://doi.org/10.1016/j.tecto.2022.229655.

Di Bucci, D., Mazzoli, S., 2002. Active tectonics of the Northern Apennines and Adria geodynamics: new data and a discussion. J. Geodyn. 34 (5), 687–707. https://doi.org/10.1016/S0264-3707(02)00107-2.

Discenza, M.E., Esposito, C., Di Luzio, E., Delchiaro, M., Di Martire, D., Minnillo, M., Mugnozza, G.S., 2023. Deep-Seated Gravitational Slope Deformations in Molise region (Italy): novel inventory and main geomorphological features. J. Maps 1–14. https://doi.org/10.1080/17445647.2022.2163198.

Fawcett, T., 2006. An introduction to ROC analysis. Pattern recognition letters 27 (8), 861–874. https://doi.org/10.1016/j.patrec.2005.10.010.

Friedman, J.H., 1991. Multivariate adaptive regression splines. Ann. Stat. 19 (1), 1–67. https://doi.org/10.1214/aos/1176347963.
Generali, M., Pizziolo, M., 2013. The Susceptibility Map for Landslides with Shallow Initiation in the Emilia Romagna Region (Italy). In: Margottini, C., Canuti, P., Sassa, K. (Eds.), Landslide Science and Practice. Springer, Berlin, Heidelberg. https://doi.org/10.1007/978-3-642-31325-7_57.
Ghiselli, A., Merazzi, M., Strini, A., Margutti, R., Mercuriali, M., 2011. Hypogeal geological survey in the "Grotta del Re Tiberio" natural cave (Apennines, Italy): a valid tool for reconstructing the structural setting. Open Geosci 3 (2), 155–168. https://doi.org/10.2478/s13533-011-0012-8.
Goodenough, D.J., Rossmann, K., Lusted, L.B., 1974. Radiographic applications of receiver operating characteristic (ROC) curves. Radiology 110 (1), 89–95. https://doi.org/10.1148/110.1.89.
Gorsevski, P.V., Jankowski, P., 2008. Discerning landslide susceptibility using rough sets. Comput. Environ. Urban Syst. 32 (1), 53–65. https://doi.org/10.1016/j.compenvurbsys.2007.04.001.
Gorsevski, P.V., Jankowski, P., 2010. An optimized solution of multi-criteria evaluation analysis of landslide susceptibility using fuzzy sets and Kalman filter. Comput. Geosci. 36 (8), 1005–1020. https://doi.org/10.1016/j.cageo.2010.03.001.
Gunderson, K.L., Pazzaglia, F.J., Picotti, V., Anastasio, D.A., Kodama, K.P., Rittenour, T., Frankel, K.F., Ponza, A., Berti, C., Negri, A., Sabbatini, A., 2014. Unraveling tectonic and climatic controls on synorogenic growth strata (Northern Apennines, Italy). GSA Bull 126 (3–4), 532–552. https://doi.org/10.1130/B30902.1.
Guzzetti, F., Carrara, A., Cardinali, M., Reichenbach, P., 1999. Landslide hazard evaluation: a review of current techniques and their application in a multi-scale study, Central Italy. Geomorphology 31 (1–4), 181–216. https://doi.org/10.1016/S0169-555X(99)00078-1.
Guzzetti, F., Reichenbach, P., Cardinali, M., Galli, M., Ardizzone, F., 2005. Probabilistic landslide hazard assessment at the basin scale. Geomorphology 72 (1–4), 272–299. https://doi.org/10.1016/j.geomorph.2005.06.002.
Hosmer, D.W., Lemeshow, S., 2000. Applied logistic regression. Wiley series in probability and statistics. Wiley, New York.
Huabin, W., Gangjun, L., Weiya, X., Gonghui, W., 2005. GIS-based landslide hazard assessment: an overview. Progress in Physical geography 29 (4), 548–567. https://doi.org/10.1191/0309133305pp462ra.
Huang, F., Cao, Z., Guo, J., Jiang, S.H., Li, S., Guo, Z., 2020. Comparisons of heuristic, general statistical and machine learning models for landslide susceptibility prediction and mapping. Catena 191, 104580. https://doi.org/10.1016/j.catena.2020.104580.
Huang, Y., Zhao, L., 2018. Review on landslide susceptibility mapping using support vector machines. Catena 165 (2018), 520–529. https://doi.org/10.1016/j.catena.2018.03.003.
Ilia, I., Tsangaratos, P., 2016. Applying weight of evidence method and sensitivity analysis to produce a landslide susceptibility map. Landslides 13, 379–397. https://doi.org/10.1007/s10346-015-0576-3.
Kuhn, M., 2016. A Short Introduction to the caret Package. R Found Stat Comput 1, 1–10.
Kutlug Sahin, E., Ipbuker, C., Kavzoglu, T., 2017. Investigation of automatic feature weighting methods (Fisher, Chi-square and Relief-F) for landslide susceptibility mapping. Geocarto Int 32 (9), 956–977. https://doi.org/10.1080/10106049.2016.1170892.
Lasko, T.A., Bhagwat, J.G., Zou, K.H., Ohno-Machado, L., 2005. The use of receiver operating characteristic curves in biomedical informatics. Journal of biomedical informatics 38 (5), 404–415. https://doi.org/10.1016/j.jbi.2005.02.008.
Lee, S., Choi, J., 2004. Landslide susceptibility mapping using GIS and the weight-of-evidence model. Int. J. Geogr. Inf. Sci. 18 (8), 789–814. https://doi.org/10.1080/13658810410001702003.
Lee, C.T., Huang, C.C., Lee, J.F., Pan, K.L., Lin, M.L., Dong, J.J., 2008. Statistical approach to storm event-induced landslides susceptibility. Nat. Hazards Earth Syst. Sci. 8 (4), 941–960. https://doi.org/10.5194/nhess-8-941-2008.
Lee, S., Pradhan, B., 2007. Landslide hazard mapping at Selangor, Malaysia using frequency ratio and logistic regression models. Landslides 4 (1), 33–41. https://doi.org/10.1007/s10346-006-0047.
Lombardo, L., Cama, M., Conoscenti, C., Märker, M., Rotigliano, E., 2015. Binary Logistic Regression versus Stochastic Gradient Boosted Decision Trees in Assessing Landslide Susceptibility for Multiple-Occurring Landslide Events: Application to the 2009 Storm Event in Messina (Sicily, Southern Italy). Nat. Hazards 79, 1621–1648. https://doi.org/10.1007/s11069-015-1915-3.
Lombardo, L., Bachofer, F., Cama, M., Märker, M., Rotigliano, E., 2016. Exploiting Maximum Entropy method and ASTER data for assessing debris flow and debris slide susceptibility for the Giampilieri catchment (north-eastern Sicily, Italy). Earth Surf Proc Land 41, 1776–1789. https://doi.org/10.1002/esp.3998.
Martinello, C., Cappadonia, C., Conoscenti, C., Agnesi, V., Rotigliano, E., 2021. (2021. Optimal Slope Units Partitioning in Landslide Susceptibility Mapping. J Maps 17, 152–162. https://doi.org/10.1080/17445647.2020.1805807.
Martinello, C., Cappadonia, C., Conoscenti, C., Rotigliano, E., 2022. 2022a) Landform Classification: A High-Performing Map-ping Unit Partitioning Tool for Landslide Susceptibility Assessment—a Test in the Imera River Basin (Northern Sicily, Italy. Landslides 19, 539–553. https://doi.org/10.1007/s10346-021-01781-8.
Martinello, C.; Bufalini, M.; Cappadonia, C.; Rotigliano, E.; Materazzi, M. (2023a). Combining multi-typologies landslide susceptibility maps: a case study for the Visso area (central Italy). J. Maps 2023, 19 (1), 2198148. https://doi.org/10.1080/17445647.2023.2198148.
Martinello, C., Mercurio, C., Cappadonia, C., Hernández Martínez, M.Á., Reyes Martínez, M.E., Rivera Ayala, J.Y., Conoscenti, C., Rotigliano, E., 2022. Investigating Limits in Exploiting Assembled Landslide Inventories for Calibrating Regional Susceptibility Models: A Test in Volcanic Areas of El Salvador. Appl. Sci. (Switzerland) 12. https://doi.org/10.3390/app12126151.
Martinello, C., Mercurio, C., Cappadonia, C., Bellomo, V., Conte, A., Mineo, G., Di Frisco, G., Azzara, G., Bufalini, M., Materazzi, M., Rotigliano, E., 2023. Using Public Landslide Inventories for Landslide Susceptibility Assessment at the Basin Scale: Application to the Torto River Basin (Central-Northern Sicily, Italy). Appl. Sci. 2023 (13), 9449. https://doi.org/10.3390/app13169449.
Martinello, C., Cappadonia, C., Rotigliano, E., 2023. (2023c) Investigating the Effects of Cell Size in Statistical Landslide Susceptibility Modelling for Different Landslide Typologies: A Test in Central-Northern Sicily. Appl. Sci. 13, 1145. https://doi.org/10.3390/app13021145.
Mercurio, C., Martinello, C., Rotigliano, E., Argueta-Platero, A.A., Reyes-Martínez, M.E., Rivera-Ayala, J.Y., Conoscenti, C., 2021. Mapping Susceptibility to Debris Flows Triggered by Tropical Storms: A Case Study of the San Vicente Volcano Area (El Salvador, CA). Earth 2 (1), 66–85. https://doi.org/10.3390/earth2010005.
Mercurio, C., Calderón-Cucunuba, L.P., Argueta-Platero, A.A., Azzara, G., Cappadonia, C., Martinello, C., Rotigliano, E., Conoscenti, C., 2023. Predicting Earthquake-Induced Landslides by Using a Stochastic Modeling Approach: A Case Study of the 2001 El Salvador Coseismic Landslides. ISPRS Int. J. Geo Inf. 12, 178. https://doi.org/10.3390/ijgi12040178.
Milborrow S. (2021). Derived from mda:mars by Trevor Hastie and Rob Tibshirani. Uses Alan Miller's Fortran utilities with Thomas Lumley's leaps wrapper. earth: Multivariate Adaptive Regression Splines. R package version 5.3.1. https://CRAN.R-project.org/package=earth.
Mergili, M., Marchesini, I., Rossi, M., Guzzetti, F., Fellin, W., 2014. Spatially distributed three-dimensional slope stability modelling in a raster GIS. Geomorphology 206, 178–195. https://doi.org/10.1016/j.geomorph.2013.10.008.
Montgomery, D.R., Dietrich, W.E., 1994. A physically based model for the topographic control on shallow landsliding. Water resources research 30 (4), 1153–1171. https://doi.org/10.1029/93WR02979.
Montrasio, L., Valentino, R., Losi, G., 2012. Shallow landslides triggered by rainfalls: modeling of some case histories in the Reggiano Apennine (Emilia Romagna Region, Northern Italy). Nat. Hazards 60, 1231–1254. https://doi.org/10.1007/s11069-011-9906-5.
Nistor, M.M., 2016. Spatial distribution of climate indices in the Emilia-Romagna region. Metereol. Appl. 23 (2), 304–313. https://doi.org/10.1002/met.1555.
Ohlmacher, G.C., 2007. Plan Curvature and Landslide Probability in Regions Dominated by Earth Flows and Earth Slides. Eng. Geol. 91, 117–134. https://doi.org/10.1016/j.enggeo.2007.01.005.
Pandey, A., Shekhar Sarkar, M., Palni, S., Parashar, D., Singh, G., Kaushik, S., Chandra, N., et al., 2023. Multivariate statistical algorithms for landslide susceptibility assessment in Kailash Sacred landscape, Western Himalaya. Geomatics. Nat. Hazards Risk 14, 1. https://doi.org/10.1080/19475705.2023.2227324.
Parise, M., & Jibson, R. W. (2000). A seismic landslide susceptibility rating of geologic units based on analysis of characteristics of landslides triggered by the 17 January, 1994 Northridge, California earthquake. *Engineering geology*, *58*(3-4), 251-270. https://doi.org/10.1016/S0013-7952(00)00038-7.
Piacentini, D., Troiani, F., Soldati, M., Notarnicola, C., Savelli, D., Schneiderbauer, S., Strada, C., 2012. Statistical analysis for assessing shallow-landslide susceptibility in South Tyrol (south-eastern Alps, Italy). Geomorphology 151, 196–206. https://doi.org/10.1016/j.geomorph.2012.02.003.
Piacentini, D., Troiani, F., Daniele, G., Pizziolo, M., 2018. Historical geospatial database for landslide analysis: the Catalogue of Landslide OCcurrences in the Emilia-Romagna Region (CLOCkER). Landslides 15, 811–822. https://doi.org/10.1007/s10346-018-0962-8.
Picotti, V., Pazzaglia, F.J., 2008. A new active tectonic model for the construction of the Northern Apennines mountain front near Bologna (Italy). Journal of Geophysical Research Solid. Earth 113 (B8). https://doi.org/10.1029/2007JB005307.
Pizziolo, M., Bernardi, M., Daniele, G., Generali, M., Piacentini, D., 2014. In: Lollino, G., Manconi, A., Guzzetti, F., Culshaw, M., Bobrowsky, P., Luino, F. (Eds.), Engineering Geology for Society and Territory, 5. Springer, Cham. https://doi.org/10.1007/978-3-319-09048-1_151.
Pondrelli, S., Salimbeni, S., Ekström, G., Morelli, A., Gasperini, P., Vannucci, G., 2006. The Italian CMT dataset from 1977 to the present. Phys. Earth Planet. In. 159 (3–4), 286–303. https://doi.org/10.1016/j.pepi.2006.07.008.
Ponza, A., Pazzaglia, F.J., Picotti, V., 2010. Thrust-fold activity at the mountain front of the Northern Apennines (Italy) from quantitative landscape analysis. Geomorphology 123 (3–4), 211–231. https://doi.org/10.1016/j.geomorph.2010.06.008.
Pourghasemi, H.R., Rahmati, O., 2018. Prediction of the landslide susceptibility: Which algorithm, which precision? Catena 162, 177–192. https://doi.org/10.1016/j.catena.2017.11.022.
Pradhan, B., 2010. Landslide Susceptibility mapping of a catchment area using frequency ratio, fuzzy logic and multivariate logistic regression approaches. J. Indian Soc. Remote Sens. (June 2010) 38, 301– 320.
Reichenbach, P., Rossi, M., Malamud, B.D., Mihir, M., Guzzetti, F., 2018. A review of statistically-based landslide susceptibility models. Earth-science reviews 180, 60–91. https://doi.org/10.1016/j.earscirev.2018.03.001.
Ripley, B.D., 1996. *Pattern recognition and neural networks*. Cambridge university press.
Roering, J. J., Kirchner, J. W., Sklar, L. S., & Dietrich, W. E. (2001). Hillslope evolution by nonlinear creep and landsliding: An experimental study. *Geology*, *29*(2), 143-146. https://doi.org/10.1130/0091-7613(2001)029%3C0143:HEBNCA%3E2.0.CO;2.
Rotigliano, E., Agnesi, V., Cappadonia, C., Conoscenti, C., 2011. The Role of the Diagnostic Areas in the Assessment of Landslide Susceptibility Models: A Test in the

Sicilian Chain. Nat. Hazards 58, 981–999. https://doi.org/10.1007/s11069-010-9708-1.
Rotigliano, E., Martinello, C., Agnesi, V., Conoscenti, C., 2018. Evaluation of Debris Flow Susceptibility in El Salvador (CA): A Comparison between Multivariate Adaptive Regression Splines (MARS) and Binary Logistic Regression (BLR). Hungarian Geograph. Bull. 67, 361–373. https://doi.org/10.15201/hungeobull.67.4.5.
Rotigliano, E., Martinello, C., Hernandéz, M.A., Agnesi, V., Conoscenti, C., 2019. Predicting the Landslides Triggered by the 2009 96E/Ida Tropical Storms in the Ilopango Caldera Area (El Salvador, CA): Optimizing MARS-Based Model Building and Validation Strategies. Environ. Earth Sci. 78. https://doi.org/10.1007/s12665-019-8214-3.
Rouhi, J., Delchiaro, M., Della Seta, M., Martino, S., 2019. Emplacement kinematics of the Seymareh Rock-Avalanche Debris (Iran) inferred by field and remote surveying Ital. J. Eng. Geol. Environ. 99–104. https://doi.org/10.4408/IJEGE.2019-01.S-16.
Rouhi, J., Delchiaro, M., Della Seta, M., Martino, S., 2022. New insights on the emplacement kinematics of the Seymareh landslide (Zagros Mts., Iran) through a novel spatial statistical approach. Front. Earth Sci. 10, 869391. https://doi.org/10.3389/feart.2022.869391.
Serpelloni, E., Anzidei, M., Baldi, P., Casula, G., Galvini, A., 2005. Crustal velocity and strain-rate fields in Italy and surrounding regions: New results from the analysis of permanent and non-permanent GPS networks. Geophys. J. Int. 161 (3), 861–880. https://doi.org/10.1111/j.1365-246X.2005.02618.x.
Sun, D., Wen, H., Wang, D., Xu, J., 2020. A random forest model of landslide susceptibility mapping based on hyperparameter optimization using Bayes algorithm. Geomorphology 362, 107201. https://doi.org/10.1016/j.geomorph.2020.107201.
Tanyaş, H., Görüm, T., Fadel, I., Yıldırım, C., Lombardo, L., 2022. An open dataset for landslides triggered by the 2016 Mw 7.8 Kaikōura earthquake, New Zealand. Landslides 19 (6), 1405–1420. https://doi.org/10.1007/s10346-022-01869-9.
Tanyaş, H., Görüm, T., Kirschbaum, D., Lombardo, L., 2022. Could road constructions be more hazardous than an earthquake in terms of mass movement? Nat. Hazards 112 (1), 639–663. https://doi.org/10.1007/s11069-021-05199-2.
Tellini, C., Chelli, A., 2003. Ancient and recent landslide occurrences in the Emilia Apennines (Northern Apennines, Italy). Proceedings of Workshop "Geomorphological sensitivity and system response", Camerino-Modena Apennines (Italy), July 4th–9th, 2003, pp 104–114.
Tien Bui, D., Tuan, T.A., Klempe, H., Pradhan, B., Revhaug, I., 2016. Spatial prediction models for shallow landslide hazards: a comparative assessment of the efficacy of support vector machines, artificial neural networks, kernel logistic regression, and logistic model tree. Landslides 13, 361–378. https://doi.org/10.1007/s10346-015-0557-6.
Triglia, A., Iadanza, C., Bussettini, M., Lastoria, B., Barbano, A., 2015. Dissesto idrogeologico in Italia: pericolosità e indicatori di rischio. Rapporto 2015. ISPRA, Rapporti 233/2015, Rome.
Van Westen, Castellanos, E., Kuriakose, S.L., 2008. Spatial data for landslide susceptibility, hazard, and vulnerability assessment: An overview. Engineering geology 102 (3–4), 112–131. https://doi.org/10.1016/j.enggeo.2008.03.010.
Vargas-Cuervo, G., Rotigliano, E., Conoscenti, C., 2019. Prediction of Debris-Avalanches and -Flows Triggered by a Tropical Storm by Using a Stochastic Approach: An Application to the Events Occurred in Mocoa (Colombia) on 1 April 2017. Geomorphology 339, 31–43. https://doi.org/10.1016/j.geomorph.2019.04.023.
Vorpahl, P., Elsenbeer, H., Märker, M., Schröder, B., 2012. How can statistical models help to determine driving factors of landslides? Ecol. Model. 239, 27–39. https://doi.org/10.1016/j.ecolmodel.2011.12.007.
Wegmann, K.W., Pazzaglia, F.J., 2009. Late Quaternary fluvial terraces of the Romagna and Marche Apennines, Italy: Climatic, lithologic, and tectonic controls on terrace genesis in an active orogen. Quat. Sci. Rev. 28 (1–2), 137–165. https://doi.org/10.1016/j.quascirev.2008.10.006.
Yilmaz, I., 2009. Landslide susceptibility mapping using frequency ratio, logistic regression, artificial neural networks and their comparison: a case study from Kat landslides (Tokat—Turkey). Comput. Geosci. 35 (6), 1125–1138. https://doi.org/10.1016/j.cageo.2008.08.007.
Youden, W. J. (1950). Index for rating diagnostic tests. *Cancer*, *3*(1), 32-35. https://doi.org/10.1002/1097-0142(1950)3:1%3C32::AID-CNCR2820030106%3E3.0.CO;2-3.
Zhao, P., Masoumi, Z., Kalantari, M., Aflaki, M., Mansourian, A., 2022. A GIS-based landslide susceptibility mapping and variable importance analysis using artificial intelligent training-based methods. Remote Sens. (Basel) 14 (1), 211. https://doi.org/10.3390/rs14010211.
Zhou, C., Yin, K., Cao, Y., Ahmed, B., Li, Y., Catani, F., Pourghasemi, H.R., 2018. Landslide susceptibility modeling applying machine learning methods: A case study from Longju in the Three Gorges Reservoir area, China. Comput. Geosci. 112, 23–37. https://doi.org/10.1016/j.cageo.2017.11.019.